



*Supplement of*

## **Global and regional impacts of land cover changes on isoprene emissions derived from spaceborne data and the MEGAN model**

**Beata Opacka et al.**

*Correspondence to:* Beata Opacka (beata.opacka@aeronomie.be) and Jean-François Müller (jfm@aeronomie.be)

The copyright of individual parts of the supplement might differ from the article licence.

# Content

1. PFT classes and the corresponding isoprene basal emission factors in MEGANv2 (Table S1)
2. Diagram of consecutive transformations applied on LULC datasets (Figure S1)
3. Distributions of the climate zones and C3/C4 photosynthetic pathways (Table S2; Figure S2)
4. Tree cover trends at global and regional scales (2001-2016) (Table S3-S5)
5. Differences in TC and global annual isoprene emissions in 2001 (Figure S3)
6. Effects of soil moisture stress and CO<sub>2</sub> inhibition on global emissions and trends (Table S6)
7. Meteorological trends from ERA Interim (Figure S4-S5)
8. Burnt biomass VOC (Figure S6-S7)
9. Interannual variability (Figure S8)
10. Selected regions for evaluation (Figure S9)
11. Seasonal variability in Southeastern US and South China (Figure S10)
12. References

## 1 PFT classes and the corresponding isoprene basal emission factors in MEGANv2

	PLANT FUNCTIONAL TYPES		EMISSION FACTORS in $\mu\text{g m}^{-2}\text{h}^{-1}$
TREES	1.	Needleleaf Evergreen, Temperate	600
	2.	Needleleaf Evergreen, Boreal	3,000
	3.	Needleleaf Deciduous, Boreal	1
	4.	Broadleaf Evergreen, Tropical	7,000
	5.	Broadleaf Evergreen, Temperate	10,000
	6.	Broadleaf Deciduous, Tropical	7,000
	7.	Broadleaf Deciduous, Temperate	10,000
	8.	Broadleaf Deciduous, Boreal	11,000
SHRUBS	9.	Broadleaf Evergreen, Temperate	2,000
	10.	Broadleaf Deciduous, Temperate	4,000
	11.	Broadleaf Deciduous, Boreal	4,000
GRASS	12.	C3 Arctic Grass	1,600
	13.	C3 non-Arctic Grass	800
	14.	C4 Grass	200
CROP	15.	Crop	1

Table S1: The 16 plant functional types compatible with the Community Land Model (CLM) used in MEGANv2.

## 2 Diagram of consecutive transformations applied on LULC datasets

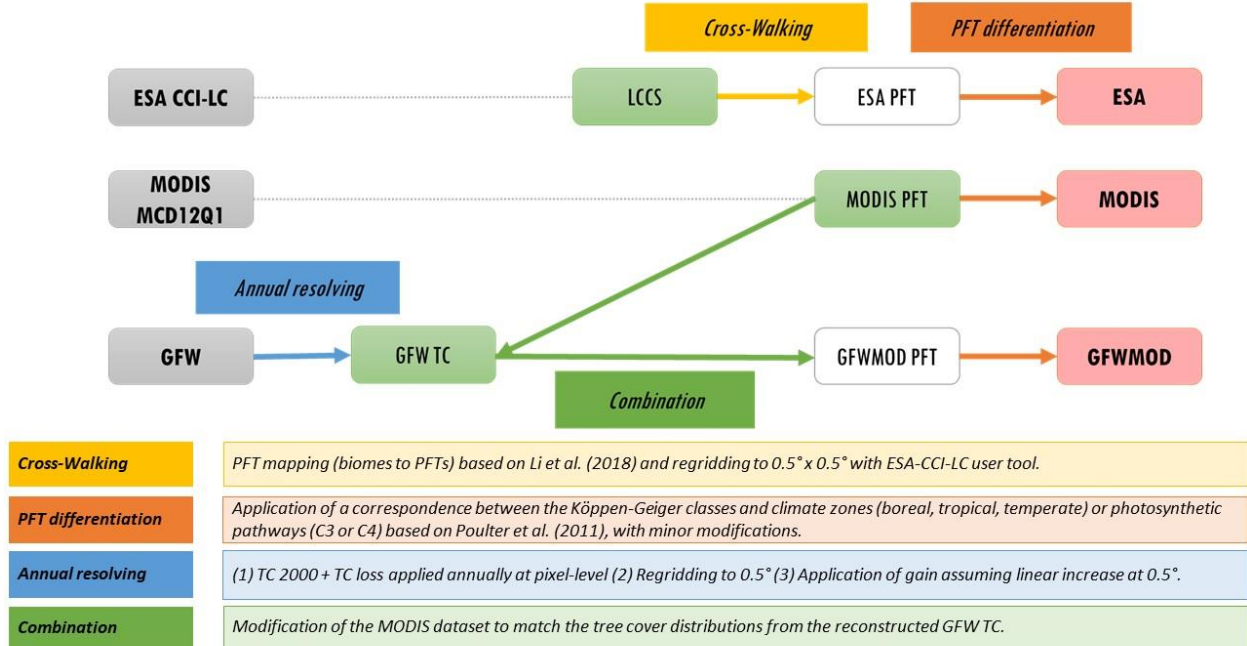


Figure S1: Schematic representation of the consecutive transformations applied on the original datasets (in grey boxes) to generate annually updated LULC maps comprising 16 PFTs, compatible with the MEGAN model (in red boxes). Initial (annually resolved) and intermediate maps are in green and white boxes, respectively. Transformations are represented by arrows with a short description inset.

### 3 Distributions of the climate zones and C3/C4 photosynthetic pathways

The differentiation into climate zones and photosynthetic pathways applied on trees, shrubs and grasses was performed based on Table 3 from Poulter et al. (2011). A few adjustments were applied on their Table 3. The updated Köppen-Geiger classes are listed in Table S2. Classes ‘Dfa’ and ‘Dfb’ were reclassified as temperate instead of boreal types because the boreal ecoregion was protruding southward over Eastern Europe and North-East USA, below the established transition latitude at about 50° N (Hall et al., 2004). Besides, certain C3 (classified as ‘cool’ in Table 3) and C4 (‘warm’ in Table 3) classes have been interchanged (‘BWk’, ‘BSk’, ‘Csa’, ‘Dwa’, ‘Dfb’) for a better agreement with the literature on the topic (Woodward et al., 2004; Shoko et al., 2016) and the CLM map, for which the mapping method of Still was applied using MODIS LAI (Still et al., 2003; Lawrence and Chase, 2007). In reality, certain regions are prone to the co-existence of C3 and C4 grasses species, but no mixed grassland is accounted for in this study. The original and modified distributions of biomes are shown in Figure S1.

	ORIGINAL	MODIFIED
TROPICAL	---	---
TEMPERATE		Dfa, Dfb
BOREAL	Dfa, Dfb	
WARM C4	BWk, BSk, Csa, Dwa	
COOL C3		BWk, BSk, Csa, Dfb
ARCTIC C3	Dfb	Dwa

Table S2: Correspondence between Köppen-Geiger classes and biomes/photosynthetic pathways that were reclassified for the present study. The original classification as in Table 3 of Poulter et al. (2011) is given in the second column; and the modified classification is given in the third column.

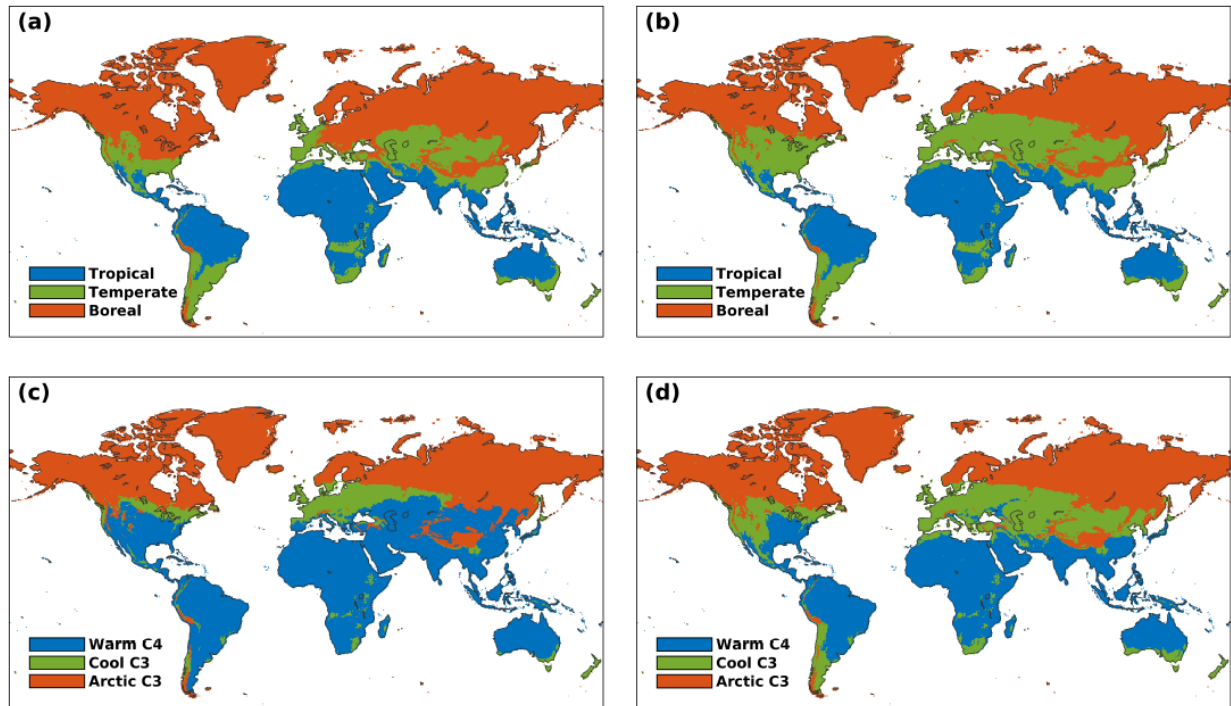


Figure S2: Differentiation according to climate zones (a: original, b: modified) and C3/C4 photosynthetic pathways (c: original, d: modified).

The mapping method used for the subdivision of PFTs into climate zones and C3/C4 classes in the CLM map differ from the method described hereinabove (see Section 15.3.3 of Oleson et al., 2010). The difference could be evaluated by aggregating classes of the CLM map with common physiognomy, leaves and phenology (i.e. NET, NDT, BET, BDT, grass and shrub) and by applying our method. The resulting sub-classes were compared to the original sub-classes. Overall, except for the grass sub-classes, little differences were seen in other vegetation types (that is NET, NDT, BET, BDT and shrub). Our method for climate subdivision based on Poulter et al. (2011) and the method of Nemani and Running (1996) gave very similar results. For the C3/C4 grass types, our method led to more warm C4 grass in the Central U.S., eastern coast of Brazil and Uruguay, Sub-Saharan Africa, eastern Australia, and South-East China. But these changes have negligible impact on global isoprene emissions given the very low basal emission factors of grass PFTs.

#### 4 Tree cover trends at global and regional scales (2001-2016)

<b>UNITS:</b> <b>km<sup>2</sup> yr<sup>-1</sup></b>	<b>MODIS</b>	<b>ESA</b>	<b>GFWMOD</b>	<b>FAOSTAT</b>
<b>TROPICAL</b>	-14.6	-8.4	-51	---
<b>BOREAL</b>	15.1	-1.8	-21.5	---
<b>TEMPERATE</b>	18.4	1.3	-11.6	---
<b>WORLD</b>	18.2	-14	-83.5	-49.7

**Table S3: Zonal and global tree cover trends (in  $\times 10^3$  km<sup>2</sup> yr<sup>-1</sup>) for the 2001-2016 period. The climate domains (tropical, temperate and boreal) were defined in Section 2.2.1. and shown in Figure S1.**

<b>UNITS:</b> <b>km<sup>2</sup> yr<sup>-1</sup></b>	<b>US</b>	<b>BRAZIL</b>	<b>CHINA</b>	<b>INDONESIA</b>	<b>RUSSIA</b>
<b>FAOSTAT</b>	4.4	-32.2	22.3	-3.9	4
<b>MODIS</b>	-2.2	-10.6	8.8	-0.8	9.3
<b>ESA</b>	-0.9	-0.9	-0.3	-2.5	0.03
<b>GFWMOD</b>	-6.6	-16.9	-2.5	-7.3	-7.7

**Table S4: Net total trends (in  $\times 10^3$  km<sup>2</sup> yr<sup>-1</sup>) for the 2001-2016 of countries with large forested areas as provided by FAOSTAT, MODIS, ESA and GFWMOD.**

Countries	Area (km <sup>2</sup> )	ABSOLUTE TRENDS ( $\times 10^3$ km <sup>2</sup> yr <sup>-1</sup> )			RELATIVE TRENDS (% yr <sup>-1</sup> )		
		MODISPFT	ESA	GFWMOD	MODISPFT	ESA	GFWMOD
Angola	1,256,855.59	-1.496	0.126	-0.910	-0.18	0.04	-0.23
Belgium	30,649.47	-0.052	-0.008	-0.014	-0.33	-0.18	-0.19
Bolivia	1,075,222.78	-0.741	-0.643	-2.456	-0.10	-0.12	-0.44
Central African Republic	622,876.08	0.083	0.070	-0.269	0.01	0.03	-0.09
Cameroon	467,897.51	-0.068	-0.062	-0.268	-0.02	-0.03	-0.11
Canada	9,969,191.15	4.177	-0.919	-9.265	0.08	-0.03	-0.31
Finland	344,843.09	-0.061	0.070	-0.498	-0.02	0.04	-0.32
France	559,265.18	0.518	-0.018	-0.082	0.18	-0.02	-0.06
Ghana	239,914.82	-0.509	0.070	-0.108	-0.46	0.22	-0.23
Guatemala	110,297.10	-0.062	-0.101	-0.509	-0.06	-0.16	-0.75
India	3,278,838.70	1.631	0.066	-0.374	0.28	0.02	-0.13
Ivory Coast	324,227.12	-0.351	-0.051	-0.441	-0.13	-0.11	-0.45
Laos	230,388.39	-0.198	-0.181	-0.713	-0.09	-0.18	-0.44
Liberia	98,171.91	-0.009	-0.170	-0.266	-0.01	-0.42	-0.40
Madagascar	609,613.23	-0.631	-0.024	-0.595	-0.37	-0.01	-0.46
Malaysia	348,993.09	-0.320	-0.490	-1.579	-0.11	-0.25	-0.63
Mozambique	791,828.48	-1.749	0.112	-0.754	-0.32	0.07	-0.39
Paraguay	399,186.85	-0.905	-1.593	-2.091	-0.26	-1.03	-1.29
Poland	312,764.36	0.381	0.029	-0.008	0.30	0.05	-0.01
Portugal	96,534.23	0.632	-0.012	-0.039	1.74	-0.06	-0.27
Democratic Republic of Congo	2,319,596.70	-0.690	-0.383	-3.640	-0.03	-0.03	-0.23
Sierra Leone	74,906.59	-0.030	-0.000	-0.139	-0.04	-0.00	-0.37
Sweden	456,165.64	-0.157	-0.218	-0.644	-0.05	-0.11	-0.33
Uganda	216,329.85	-0.495	0.039	-0.155	-0.37	0.16	-0.29
Vietnam	342,273.51	0.023	-0.007	-0.358	0.01	-0.01	-0.36

Table S5: Net total absolute and relative tree cover trends over 2001-2016 for a selection of 25 countries worldwide as provided by MODIS, ESA and GFWMOD along with the country area in km<sup>2</sup>.

## 5 Differences in TC and global annual isoprene emissions in 2001

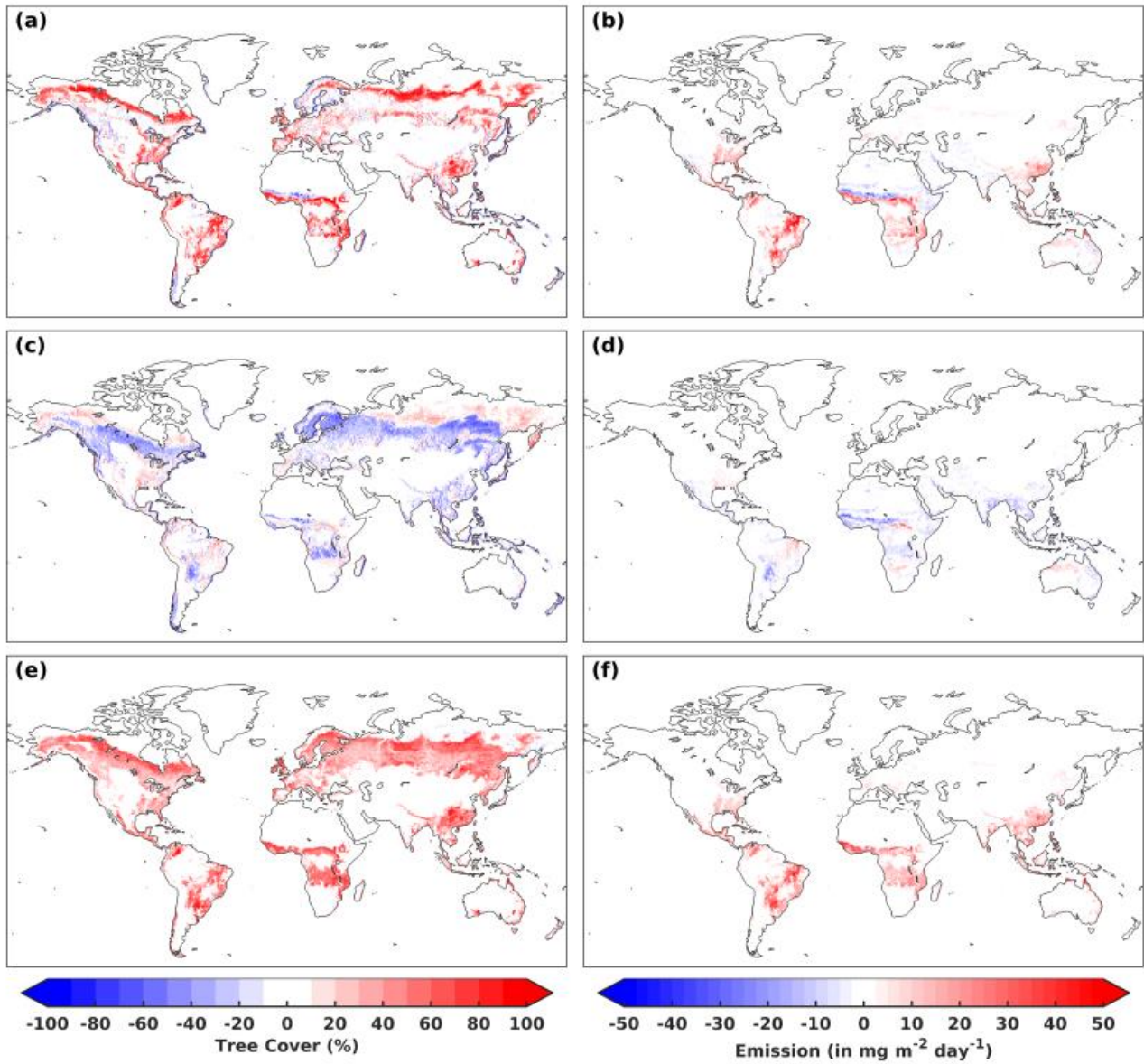


Figure S3: Differences in tree cover between the three datasets (left panels: (a) MODIS - CLM, (c) GFWMOD - CLM, and (e) MODIS - GFWMOD), and corresponding differences between the annually-averaged isoprene emissions (right panels: (b) ISOPMOD - CTRL, (d) ISOPGFW - CTRL, and (f) ISOPMOD - ISOPGFW).

## 6 Effects of soil moisture stress and CO<sub>2</sub> inhibition on global emissions and trends

		Annual mean (in Tg)			Annual trends (in %yr <sup>-1</sup> )		
		CTRL	ISOPMOD	ISOPGFW	CTRL	ISOPMOD	ISOPGFW
Standard setup	$\gamma_{SM} = 1$ $\gamma_{CO_2} = 1$	418	520	354	0.94	0.90	0.61
SM effect	<i>G12</i>	363	464	314	1.00	0.92	0.61
CO <sub>2</sub> effect	<i>PW11</i>	404	502	342	0.36	0.35	0.08
SM and CO <sub>2</sub> effects	<i>G12</i> <i>PW11</i>	351	448	304	0.46	0.42	0.12

**Table S6: Global mean annual isoprene emissions (in Tg) and trends (in % yr<sup>-1</sup>) for the 2001-2016 period in CTRL, ISOPMOD and ISOPGFW simulations. The first row shows estimations from the study run, whereas second to fourth rows show the impact of the soil moisture stress from Guenther et al. (2012) (G12) and/or the CO<sub>2</sub> inhibition following the parameterization of Possell and Hewitt (2011) (PW11).**

The CO<sub>2</sub> inhibition effect is calculated based on the mean value of annual mean concentrations measured at Mauna Loa and South Pole stations. The formulation of Possell and Hewitt (2011) for the inhibition effect leads to a small decrease of global mean isoprene emissions by 3% but the offsetting effect on trends is substantial (-0.5 %yr<sup>-1</sup>). The use of the formulation of Heald et al. (2009) would lead to an increase of global emissions by about 1.5%, with a smaller cutback on the trend compared to the aforementioned formulation (-0.2 %yr<sup>-1</sup>). The soil moisture stress defined in Guenther et al. (2012) with  $\Delta\theta_1 = 0.06$  has little effect on trends. The reduction of the global mean emissions is of the order of 10%, i.e. half of the reduction reported in the previous study of Müller et al. (2008) using MEGAN-MOHYCAN. This difference stems from the spatial differences in isoprene emissions resulting from the use of the gridded emission maps instead of using PFT maps with PFT-dependent emissions factors, as in the present study, and because of different versions of MODIS LAI products (Guenther et al., 2006; Jiang et al., 2017).



## 7 Meteorological trends from ERA Interim

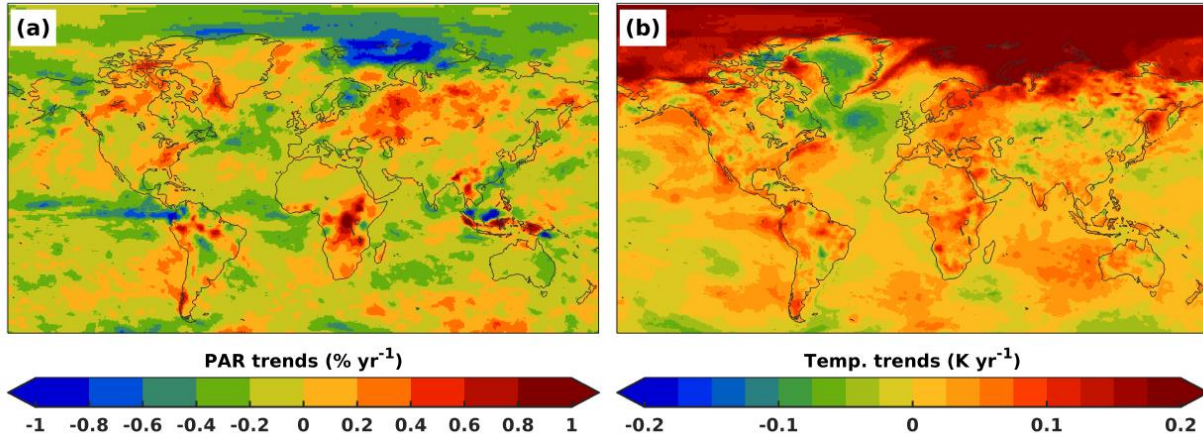


Figure S4: Distribution of trends of (a) photosynthetically active radiation (PAR, in  $\% \text{ yr}^{-1}$ ) and (b) temperature (in  $\text{K yr}^{-1}$ ) for the 2001-2016 period.

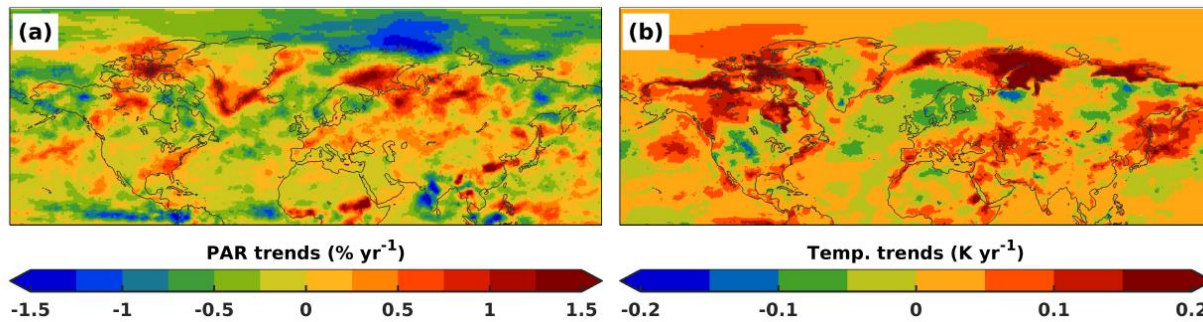


Figure S5: Distribution in trends of July-August means over the Northern Hemisphere. Despite the known Arctic-Amplification, the boreal summer trends of (a) PAR and (b) temperature conditions show a decreasing trends over 2001-2016 and is responsible of negative trends in isoprene emissions seen in Figure 7 over Siberia.

## 8 Burnt biomass VOC

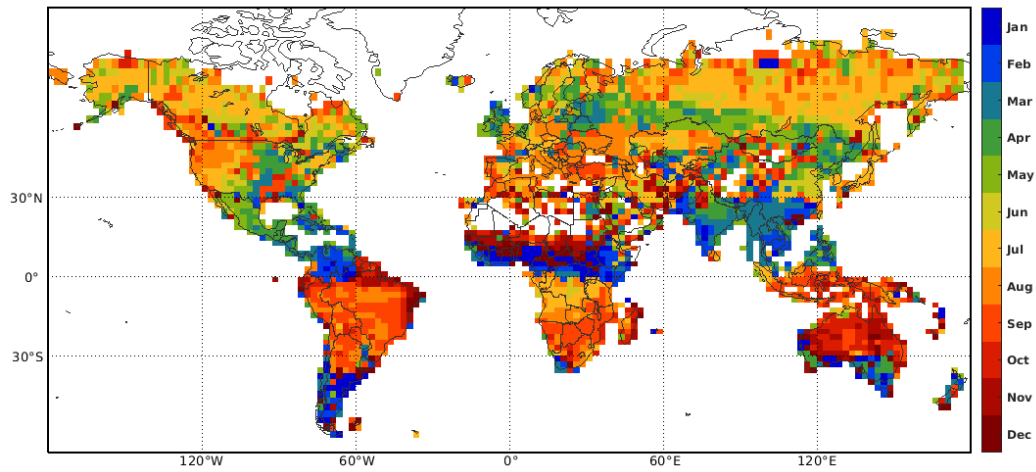


Figure S6: Middle month of the three-consecutive-month period with highest VOC emissions due to vegetation fires, based on climatological means of the GFED4s dataset for 2005-2016 (van der Werf et al., 2017) and emission factors of Andreae (2019).

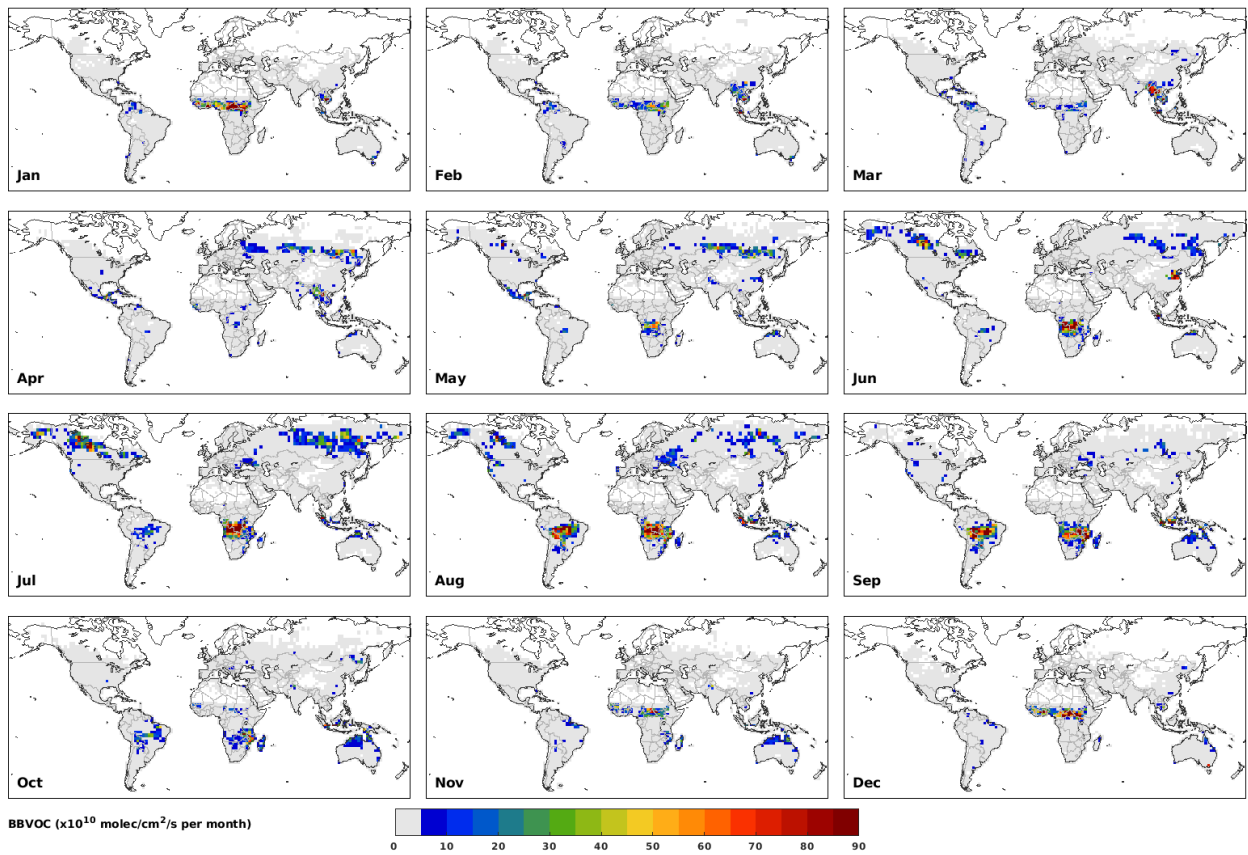


Figure S7: Monthly averaged distribution of biomass burning VOC emissions (in  $10^{10}$  molec. cm<sup>-2</sup> s<sup>-1</sup>) based on a climatology of GFED4s flux data over 2005-2016 (van der Werf et al., 2017) and emission factors of Andreae (2019).

## 9 Interannual variability

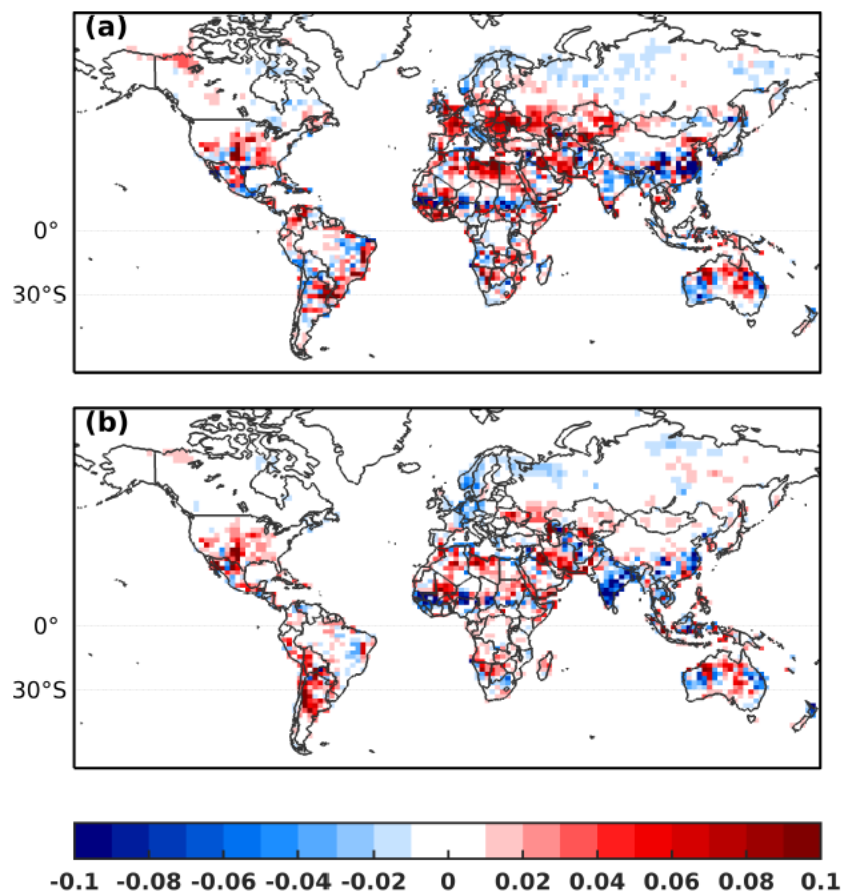


Figure S8: Difference in correlation coefficients of simulated HCHO columns with OMI HCHO columns: (a)  $R_B - R_A$  and (b)  $R_C - R_A$ , with  $R_A$ ,  $R_B$  and  $R_C$ , the correlation coefficients from run A, run B and run C, respectively.

## 10 Selected regions for evaluation

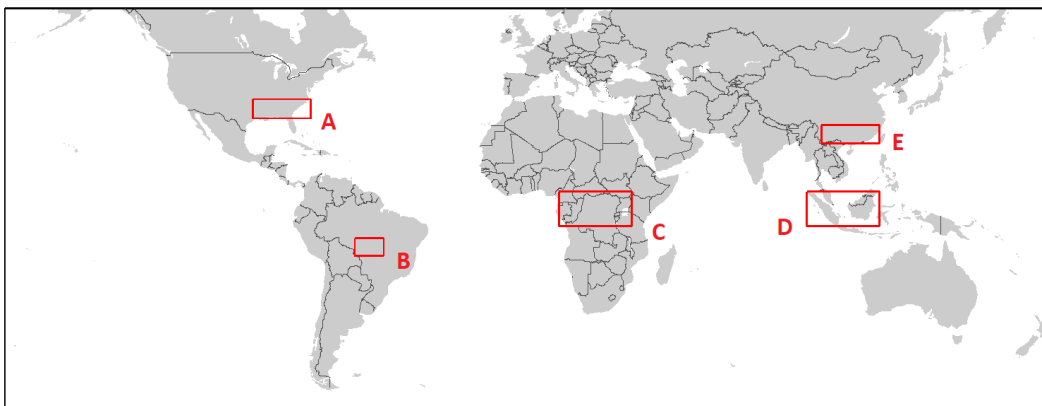


Figure S9: Map of selected regions for evaluation of HCHO interannual variability: (A) Southeastern US (30.1°-35.9° N, 77.6°-95° W), (B) Mato Grosso (10.1°-16° S, 50.1°-60°W), (C) Equatorial Africa (6°S-5.9° N, 10°-34.9° E), (D) Indonesia (5.9°S-5.9° N, 95°-119.9° E, and (E) South China (22°-27.9° N, 100°-119.9° E).

## 11 Seasonal variability in Southeastern US and South China

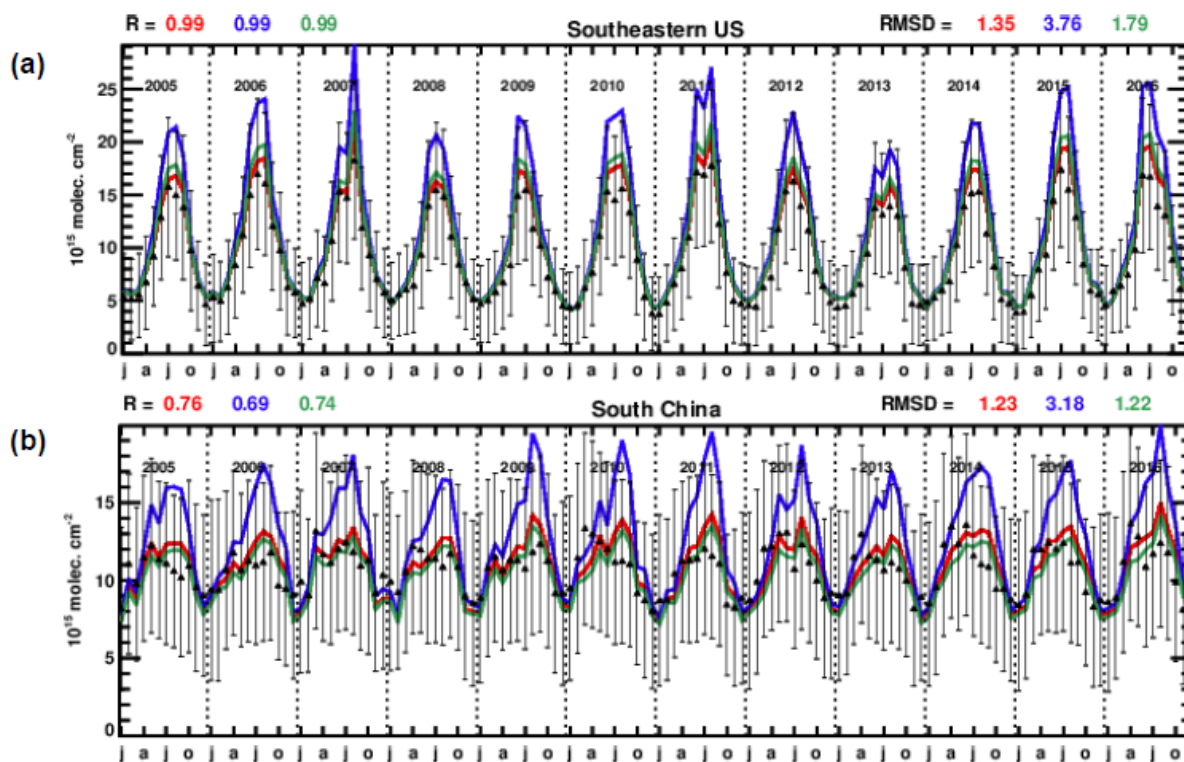


Figure S10: Time series over 2005-2016 of monthly averaged OMI HCHO columns (black triangles) and modelled HCHO over (a) Southeastern US and (b) South China. The error bars represent the estimated OMI column uncertainties. The solid lines represent the model-calculated columns from runs A (red), B (blue) and C (green). The correlation coefficient (R) and the root-mean square deviations (RMSD) are given inset.

## 12 References

- Andreae, M.O.: Emission of trace gases and aerosols from biomass burning—an updated assessment, *Atmos. Chem. Phys.*, 19, 8523-8546, doi: 10.5194/acp-19-8523-2019, 2019.
- Guenther, A. B., Karl, T., Harley, P., Wiedinmyer, C., Palmer, P. I., and Geron, C.: Estimates of global terrestrial isoprene emissions using MEGAN (Model of Emissions of Gases and Aerosols from Nature), *Atmos. Chem. Phys.*, 6, 3181-3210, 2006.
- Guenther, A. B., Jiang, X., Heald, C. L., Sakulyanontvittaya, T., Duhl, T., Emmons, L. K., and Wang, X.: The Model of Emissions of Gases and Aerosols from Nature version 2.1 (MEGAN2.1): an extended and updated framework for modeling biogenic emissions, *Geosci. Model Dev.*, 5, 1471-1492, doi: 10.5194/gmd-5-1471-2012, 2012.
- Hall, F.G., Betts, A.K., Frolking, S., Brown, R., Chen, J.M., Chen, W., Halldin, S., Lettenmaier, D.P., and Schafer, J.: The boreal climate, in: *In Vegetation, Water, Humans and the Climate*, edited by: Kabat, P., Claussen, M., Dirmeyer, P. A., Gash, J. H. C., de Guenni, L. B., Meybeck, M., Pielke, R. A., Vörösmarty, C. I., Hutjes, R. W. A., and Lütke-meier, S., Springer, Berlin, Heidelberg, Germany, doi: 10.1007/978-3-642-18948-7\_8, 93-114, 2004.
- Heald, C.L., Wilkinson, M.J., Monson, R.K., Alo, C.A., Wang, G., and Guenther, A.: Response of isoprene emission to ambient CO<sub>2</sub> changes and implications for global budgets, *Glob. Chang. Biol.*, 15, 1127-1140, doi: 10.1111/j.1365-2486.2008.01802.x, 2009.
- Jiang, C., Ryu, Y., Fang, H., Myneni, R., Claverie, M., and Zhu, Z.: Inconsistencies of interannual variability and trends in long-term satellite leaf area index products, *Global Change Biol.*, 23, 4133-4146, doi: 10.1111/gcb.13787, 2017.
- Lawrence, P. J. and Chase, T. N.: Representing a new MODIS consistent land surface in the Community Land Model (CLM 3.0), *J. Geophys. Res.*, 112, G01023, doi:10.1029/2006JG000168, 2007.
- Li, W., MacBean, N., Ciais, P., Defourny, P., Lamarche, C., Bontemps, S., Houghton, R.A., and Peng, S.: Gross and net land cover changes in the main plant functional types derived from the annual ESA CCI land cover maps (1992–2015), *Earth Syst. Sci. Data*, 10, 219-234, doi: 10.5194/essd-10-219-2018, 2018.
- Müller, J.-F., Stavrou, T., Wallens, S., De Smedt, I., Van Roozendaal, M., Potosnak, M. J., Rinne, J., Munger, B., Goldstein, A., and Guenther, A. B.: Global isoprene emissions estimates using MEGAN, ECMWF analyses and a detailed canopy environment model, *Atmos. Chem. Phys.*, 8, 1329-1341, doi: 10.5194/acp-8-1329-2008, 2008.
- Nemani, R., and Running, S.W.: Implementation of a hierarchical global vegetation classification in ecosystem function models, *J. Veg. Sci.*, 7, 337-346, doi: 10.2307/3236277, 1996.
- Oleson, K.W., Lawrence, D.M., Gordon, B., Flanner, M.G., Kluzek, E., Peter, J., Levis, S., Swenson, S.C., Thornton, E., Feddema, J. and Heald, C.L.: Technical description of version 4.0 of the Community Land Model (CLM), Tech. Note NCAR/TN-478+STR, University Corporation for Atmospheric Research, Boulder, Colorado, US, doi:10.5065/D6FB50WZ, 2010.
- Possell, M., and Hewitt, C.N.: Isoprene emissions from plants are mediated by atmospheric CO<sub>2</sub> concentrations, *Glob. Change Biol.*, 17, 1595-1610, 2011.
- Poulter, B., Ciais, P., Hodson, E., Lischke, H., Maignan, F., Plummer, S., and Zimmermann, N.E.: Plant functional type mapping for earth system models, *Geosci. Model Dev.*, 4, 993-1010, doi: 10.5194/gmd-4-1-2011, 2011.
- Shoko, C., Mutanga, O. and Dube, T.: Progress in the remote sensing of C3 and C4 grass species aboveground biomass over time and space, *ISPRS J. Photogramm. Remote Sens.*, 120, 13-24, doi: 10.1016/j.isprsjprs.2017.04.016, 2016.
- Still, C.J., Berry, J.A., Ribas-Carbo, M., and Helliker, B.R.: The contribution of C 3 and C 4 plants to the carbon cycle of a tallgrass prairie: an isotopic approach., *Oecologia*, 136, 347-359, doi:10.1007/s00442-003-1274-8, 2003.

van Der Werf, G.R., Randerson, J.T., Giglio, L., Van Leeuwen, T.T., Chen, Y., Rogers, B.M., Mu, M., Van Marle, M.J., Morton, D.C., Collatz, G.J., Yokelson, R.J., and Kasibhatla, P.S.: Global fire emissions estimates during 1997-2016, *Earth Syst. Sci. Data*, 9, 697–720, doi: 10.5194/essd-9-697-2017, 2017.

Woodward, F.I., Lomas, M.R. and Kelly, C.K.: Global climate and the distribution of plant biomes. *Phil. Trans. R. Soc. B.*, 359, 1465-1476, doi: 10.1098/rstb.2004.1525, 2004.